Determination of the melting temperature of hexagonal ice using Lee-Yang phase transition theory

Ling Liu, Yihua Dong, Qi-Jun Ye,* and Xin-Zheng Li†

Interdisciplinary Institute of Light-Element Quantum Materials, Research Center for Light-Element Advanced Materials, and Collaborative Innovation Center of Quantum Matter, Peking University, Beijing 100871, People's Republic of China; State Key Laboratory for Artificial Microstructure and Mesoscopic Physics, Frontier Science Center for Nano-optoelectronics and School of Physics, Peking University, Beijing 100871, People's Republic of China; and Peking University Yangtze Delta Institute of Optoelectronics, Nantong, Jiangsu 226010, People's Republic of China

(Received 27 May 2025; revised 12 August 2025; accepted 25 August 2025; published 15 September 2025)

Lee-Yang phase transition theory is a milestone in statistical physics. Its applications in realistic systems, however, had been substantially hindered by availability of practical schemes to calculate the Lee-Yang zeros. In this manuscript, we extend the scheme we have designed earlier [Phys. Rev. E **109**, 024118 (2024)] and report simulation results for the melting temperature (T) of ice Ih under ambient pressure (p). The enhanced sampling technique is shown to be crucial for accessing Lee-Yang zeros accurately. The real and imaginary parts of the Lee-Yang edges exhibit linear finite-size scaling, yielding an extrapolated melting T of 274.70 K for the mW water potential in the thermodynamic limit. This result agrees quantitatively with prior coexistence simulations, while offering a significant reduction in computational cost: the phase boundary can be determined from a single simulation even when performed distant from actual transition conditions, unlike conventional methods that require multiple simulations scanning T or p. With these, we demonstrate the applicability of Lee-Yang phase transition theory in realistic molecular systems and provide a feasible scheme for high-throughput calculations in determining the phase transition temperature.

DOI: 10.1103/fr9q-df52

I. INTRODUCTION

Phase and phase transition rank among the most ubiquitous phenomena in nature [1–8]. Since the early days of thermodynamics, theoretical description of them has became a fundamental challenge in physics [9]. One successful model for descriptions of the phase transition is the van der Waals (vdW) model, proposed in 1873 [10]. With it, one can explain the transition of the same matter between gas and liquid phases, even before the nature of the interactions between molecules was revealed and the word of "phase" was proposed [11,12]. Starting from the beginning of the past century, phases and phase transitions have been systematically studied in magnetic systems, especially on the Ising model [13–15]. In 1952, based on theoretical analysis of the Ising model and the lattice gas model, Yang and Lee proposed a theory for descriptions of the phase transitions using the zeros of the partition function, i.e., the Lee-Yang zeros on the complex plane of the thermodynamic state functions [16,17]. This provides a beautiful mathematical framework for theoretical description of the phase transitions [18]. Applications of this theory, however, have been largely restricted to simple model systems, due to the lack of numerical scheme for calculations of the Lee-Yang zeros in realistic systems [19–24].

Parallel to understanding phase transitions using models, theoretical descriptions have also benefited from developments of molecular simulation methods since the mid-20th century [25]. The advent of computers, especially supercomputers, have enabled numerical schemes like the molecular dynamics (MD) [26,27], Monte Carlo (MC) [28,29], and first-principles electronic structures methods [30,31], transforming material science by allowing researchers to predict material properties with unprecedented precision and efficiency. In the context of phase transition studies, free-energy calculations and coexistence simulations have been the most popular methods for determining the phase boundaries. The former aims to find the thermodynamics conditions where the free energies of the competing phases are equal [32–36], while the latter relies on MD simulations that can maintain the coexistence of the competing phases, starting from a box where they are in contact [37–40]. Both methods have achieved significant success in investigations of the realistic systems, such as water-ice transitions [33,34,38,39], liquid-liquid phase transitions [35,36], and melting of high-pressure hydrogen [41,42]. Limitations of them, however, are also obvious. A prominent one is that they typically require multiple simulations under different T and p conditions, rendering the study of phase boundaries a trial-and-error process that can incur high computational costs.

In recent years, there has been a growing interest in combining molecular simulations with the calculation of Lee-Yang zeros for realistic systems. The central challenge lies in accurately determining the density of states (DOS), which is essential for calculating the partition functions. Rocha *et al.* utilized the multicanonical MC method to obtain precise estimates of the DOS in the canonical (NVT) ensemble, enabling the determination of Lee-Yang zeros for finite polymer systems [43,44]. Recently, our group designed a scheme to calculate Lee-Yang zeros from MD simulations in the isothermal–isobaric (NpT) ensemble [45], where the DOS for enthalpy is derived from its probability distribution obtained

*Contact author: qjye@pku.edu.cn
†Contact author: xzli@pku.edu.cn

 ©2025 American Physical Society

directly from the MD trajectories. We demonstrated that the projected Lee-Yang zeros in the supercritical region align well with the Widom lines (commonly interpreted as "supercritical boundaries"), while those in the phase transition region coincide with the phase coexistence line [45]. This advance implies an alternative strategy to free-energy calculations and coexistence simulations for studying phase transitions in realistic condensed matter systems. Significant numerical challenges, however, still remain, including the fact that high free-energy barriers in most phase transition processes may lead to insufficient sampling of the probability distribution. Addressing this issue requires integrating enhanced sampling methods into the framework.

In this manuscript, we report our progress in this direction, by employing the on-the-fly probability enhanced sampling (OPES) method to calculate the Lee-Yang zeros. As an example, we apply this method to study the phase transition between liquid water and ice Ih, a process that has been well studied using the free-energy methods and direct coexistence technique [33,34,38,39]. We show that the melting T of ice Ih can be determined from the Lee-Yang zeros calculated using a single OPES simulation, rather than conducting multiple simulations under varying thermodynamic conditions. This approach significantly reduces the computational cost, requiring only postprocessing of MD simulation results using Lee-Yang phase transition theory. The associated computational overhead is negligible and a PYTHON script is provided to perform the analysis. We also demonstrate excellent numerical agreement in melting T predictions, with results remaining robust against artificial parameters such as simulated temperatures and enthalpy bin size. This implies that simulations can be conducted without knowing the range of transition temperature, provided sampling efficiency is properly maintained. By extrapolating the Lee-Yang zeros to infinite system size, the real part of the Lee-Yang edge on the complex temperature plane reaches the melting T in the thermodynamic limit, while the imaginary part diminishes almost to zero. In so doing, this work presents a numerical scheme for investigating phase transitions in condensed matter systems within a single shot and without prior knowledge of phase transition.

The paper is organized as follows. In Sec. II, we give a brief introduction to the method for calculating Lee-Yang zeros using MD simulation results, introduce the collective variables used for the OPES simulations, and provide the computational details. In Sec. III, we present numerical results for determining the melting T from Lee-Yang zeros, with the effects of simulated temperatures and finite system sizes discussed. The conclusions are given in Sec. IV. For ease of implementation, a PYTHON script for calculating Lee-Yang zeros is provided as Algorithm 1 in Appendix A. Appendix B discusses the geometrical correlations between the enthalpy distribution and the zeros.

II. METHOD AND COMPUTATIONAL DETAILS

A. Lee-Yang phase transition theory

Phase transitions are characterized by the failure of an analytical function to describe a physical quantity using the state function, as abrupt changes are observed in experiments [Fig. 1(a)]. A key factor in the mathematical description of this phenomenon, which can bring such a failure of the analytical function, is the "singularity" of the thermodynamic quantities. In statistical physics, this is related to the "zero" of the "partition function" [16]. However, within the conventional understanding of the state functions, i.e., treating them as real numbers, the partition function is free of zero for all the physical thermodynamic conditions.

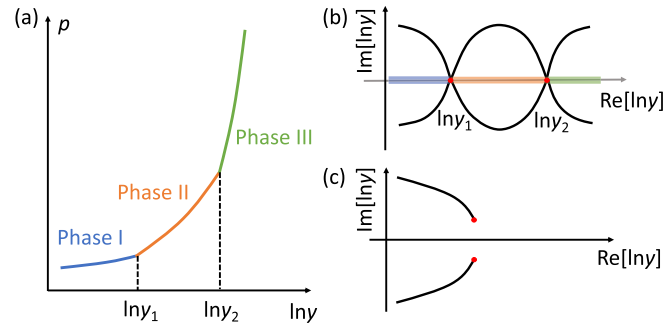

FIG. 1. Schematic representation of the Lee-Yang phase transition theory. (a) Failure of the analytical property of the pressure p as a function of ln$y$ in Eq. (3) in the case when phase transition happens at lny_1 and lny_2. (b) The distribution of the Lee-Yang zeros of ln$y$ in the complex plane of it when there are phase transitions and (c) when there is no phase transition.

Following Ref. [16], we take the lattice gas model as an example to illustrate this problem. Consider a box with fixed volume V and T, which can exchange atoms with a reservoir at a given chemical potential μ; the relative probability of having N atoms in this box is given by

$$\frac{Q_N}{N!}y^N, \tag{1}$$

where

$$Q_N = \int \cdots \int_V dr_1 dr_2 \ldots dr_N \times \exp[-U(r_1, r_2, \ldots, r_N)/(k_B T)] \tag{2}$$

and

$$y = \frac{1}{\lambda^3}\exp[\mu/(k_B T)]. \tag{3}$$

This Q_N is the configurational part of the partition function for N atoms in this box and $\lambda = (2\pi m k_B T/h^2)^{-1/2}$ is the thermal de Broglie wavelength at T. Then, the grand partition function is written as

$$Z_V = \sum_{N=0}^{M} \frac{Q_N}{N!}y^N, \tag{4}$$

where M represents the maximum number of atoms that can be contained in this box. From Eqs. (1)–(4), it is clear that, with a physical chemical potential, i.e., a real μ, the partition function Z_V is always positive. This presents a logical dilemma between conventional statistical physics—where partition function zeros are absent and thermodynamic singularities cannot exist—and our empirical observations of phase

transitions where the breakdown of analyticity plays a central role.

The genius idea of the Lee-Yang phase transition theory, as proposed in Ref. [16], is to treat the state functions, such as the ln$y$ in Fig. 1, as inherently complex rather than physically real ones. As a result, the partition function, which remains positive for real ln$y$'s, emerges zero for complex ln$y$'s. Lee and Yang demonstrated that, when the zeros of partition function approach a specific point (e.g., y_1) on the positive real axis in the thermodynamic limit, the function $p(y)$ exhibits increasingly sharp variations near y_1, ultimately leading to the emergence of singularities that signal a phase transition [Figs. 1(a) and 1(b)]. In contrast, if no zeros exist in the neighborhood of a real-valued y, $p(y)$ remains analytic in that region [Fig. 1(c)]. These zeros, known as Lee-Yang zeros, correspond to complex chemical potential μ of the lattice gas model and magnetic field of the Ising model in the original papers of Yang and Lee [16,17]. A few years later, this treatment of using complex numbers was extended to T, with the corresponding zeros called Fisher zeros [18]. We shall refer to these complex zeros collectively as Lee-Yang zeros. For clarity, we distinguish them as T zeros (Fisher zeros) or μ zeros (Lee-Yang zeros) to specify which state function is treated as complex.

Conventional theoretical studies of Lee-Yang phase transition theory have two obvious restrictions. The first one is that it was solely applied to studies of phase transition. Last year, using the van der Waals model, Ising model, and water system as examples, we demonstrated that this theory, based on Lee-Yang zeros, can also describe the supercritical matter [45]. The Lee-Yang edges, i.e., the Lee-Yang zeros closest to the real plane, locate at the complex plane but largely correspond to the Widom lines in the physical world [45]. Given the significance of supercritical regions in the phase diagram, we believe this insight will motivate further investigations into supercritical states using the Lee-Yang phase transition theory. The second one, as mentioned in the Introduction, is that they were mostly based on model systems. To address this, we developed a scheme to calculate the Lee-Yang zeros from MD simulations in our recent paper [45]. However, calculating Lee-Yang zeros remains technically difficult, posing a significant obstacle to the broader applications and extensions of the Lee-Yang phase transition theory. This challenge brings us to two key topics that will be explored in the next subsections, i.e., the scheme for calculating the Lee-Yang zeros from the MD simulations and how we improve it employing enhanced sampling techniques.

B. Calculation of Lee-Yang zeros using MD

We start from the scheme we have set up in Ref. [45]. The central idea is that the thermodynamic properties of a system should be described by complex phase diagrams, using the complex values of the state functions as its axes, rather than their real values. For example, one should employ a four-dimensional phase diagram denoted by $\tilde{T}$-$\tilde{p}$, where the tilde means complex numbers, rather than a two-dimensional one denoted by T-p. It has been shown in Ref. [45] that this complex phase diagram enables an easier geometrical description of the controversial boundaries in the conventional phase diagram. Besides the $\tilde{T}$-$\tilde{p}$ phase diagram, there can be also $\tilde{T}$-$\tilde{h}$ and $\tilde{h}$-$\tilde{p}$ ones, describing the response of this system to other state functions such as the magnetic field $\tilde{h}$. To reveal this four-dimensional phase diagram in an intuitive manner, we choose to fix one state function at a real and physical value and visualize the response of the system on the complex plane of another state function.

Taking the $\tilde{T}$-$\tilde{p}$ phase diagram as an example, we performed a series of NpT MD simulations [45]. To visualize the response of the system to T, we will fix p and treat T as a complex number $\tilde{T}$. The partition function as a function of T is written as an integral of the enthalpy H [46]:

$$Z = \int_H \rho(H) e^{-\beta H} dH. \tag{5}$$

Here, H represents an instantaneous quantity defined as $H = U + pV$, where U and V denote the instantaneous potential energy and volume sampled during the MD simulations. $\beta = 1/(k_B T)$ and $\rho(H)$ is the DOS of H. Then, the partition function in Eq. (5) is analytically continued as $Z_p(\tilde{T})$, replacing T with $\tilde{T}$ while keeping all the other terms unchanged. Similarly, to visualize the response of the system to p, we will fix T and treat p as a complex number $\tilde{p}$. The partition function turns out to be an integral of the volume V, as

$$Z = \int_V \rho(V) e^{-\beta p V} dV, \tag{6}$$

where $\rho(V)$ is the DOS of V and Z is analytically continued as $Z_T(\tilde{p})$ accordingly. The partition function Z can be reconstructed numerically, as $\rho(H)$ and $\rho(V)$ can be obtained from NpT simulations. Thus, using $Z_p(\tilde{T})$ and $Z_T(\tilde{p})$, one could analyze the structures of the partition function and the Lee-Yang zeros.

As we focus on the melting T in this work, we detail the structure of $Z_p(\tilde{T})$ and analyze the zeros of the partition function on the complex plane of $\tilde{T}$ in the following discussions, while the determination of the $\tilde{p}$ zeros follows a similar manner [45]. In this case, T becomes $\tilde{T} = T + i\tau$, with τ meaning the magnitude of its imaginary part. The aim is to search for the roots of $Z_p(\tilde{T}) = 0$. The integral in Eq. (5) will be discretized and represented as a polynomial. Using a bin size ΔH and hence $H_k = H_0 + k\Delta H$, the partition function can be rewritten as

$$Z_p(\tilde{T}) = \sum_k \rho_k e^{-\tilde{\beta} H_k} \Delta H = \Delta H \, e^{-\tilde{\beta} H_0} \sum_k \rho_k [e^{-\tilde{\beta}\Delta H}]^k. \tag{7}$$

The density of states $\rho(H)$ can be related to the probability distribution of enthalpy $g(H)$, by $\rho(H) = g(H) e^{\beta H}$. Then, we have

$$Z_p(\tilde{T}) = \Delta H \, e^{-(\tilde{\beta}-\beta) H_0} \sum_k g_k [e^{-(\tilde{\beta}-\beta)\Delta H}]^k. \tag{8}$$

Note that $g_k = g(H_k)$ is the probability distribution of H_k sampled at physical T and p. After ignoring the constant and nonzero terms, the partition function in Eq. (8) is obviously proportional to a polynomial of $y = e^{-(\tilde{\beta}-\beta)\Delta H}$, in the form of

$$Z_p(\tilde{T}) \sim \sum_k g_k y^k \sim \prod_k (y - y_k^*), \tag{9}$$

where g_k serves as the polynomial coefficient. In so doing, the roots of polynomial y_k^* can be solved numerically with a PYTHON script, provided in Appendix A.

C. Selection of collective variables

The above analysis is reliable as long as $g(H)$ converges in the NpT simulations at the target (T, p) conditions. However, this requirement has posed a significant challenge in practical MD simulations, especially for systems with complex liquid structures [33,35,47]. To this end, we employ the OPES-explore enhanced sampling method [48] to efficiently compute the enthalpy probability distributions using both the all-atom TIP4P/2005 rigid water model [49] and the coarse-grained mW potential [50].

Like all the adaptive-bias methods, appropriate collective variables (CVs) should be introduced in OPES-explore to distinguish between the liquid water and ice Ih, thereby facilitating both the crystallization and melting of the ice phase. Here, we use the Environment Similarity CV that reflects the number of icelike molecules in the simulation box [33,34], ranging from 0 to N, the total number of water molecules. The construction of this CV involves *three steps*. *First*, a similarity metric function $k_{\chi_l}(\chi)$ is defined to quantify the similarity between an environment χ around a given water and a reference environment χ_l, where

$$k_{\chi_l}(\chi) = \frac{1}{n}\sum_{i\in\chi_l}\sum_{j\in\chi}\exp\left(-\frac{|\mathbf{r}_j - \mathbf{r}_i^0|^2}{4\sigma^2}\right). \tag{10}$$

Here, $\mathbf{r}_i^0$ and $\mathbf{r}_j$ are the positions of neighboring atoms relative to the central oxygen atom in environments χ_l and χ, respectively, σ is a broadening parameter of Gaussian, and n is the total number of neighbors used for normalization. The configurations of ice Ih are generated using GenIce2 [51,52]. By inspecting these ice configurations with the Environment Finder tool [53,54], we identify four reference environments, each including 17 nearest neighbors up to the second solvation shell, with equivalent structures but different orientations.

The *second* step is to find out the best match with these four reference environments. A smooth maximum function is used to ensure the CVs are continuous and differentiable, as required in driving OPES-explore simulations, by

$$\begin{aligned} k(\chi) &= \max\left\{k_{\chi_1}(\chi), k_{\chi_2}(\chi), k_{\chi_3}(\chi), k_{\chi_4}(\chi)\right\} \\ &\approx \frac{1}{\lambda}\ln\left(\sum_{l=1}^{4}\exp[\lambda k_{\chi_l}(\chi)]\right). \end{aligned} \tag{11}$$

Here, λ is set to 100 to make the smooth approximation solid. The Gaussian broadening σ is set to 0.052 Å to make a well separation of ice-like and non-ice-like molecules in the $k(\chi)$ distribution [33]. *Third*, the similarity CV (N_{ice}) is defined as the number of ice-like molecules which satisfy $k(\chi^i) > \kappa$, where χ^i is the environment of water i and the threshold κ is set to 0.5 based on the $k(\chi)$ distribution [33]. Using the formula of a switching function, N_{ice} can be expressed as

$$N_{\text{ice}} = N - \sum_{i=1}^{N}\frac{1-[k(\chi^i)/\kappa]^n}{1-[k(\chi^i)/\kappa]^m}, \tag{12}$$

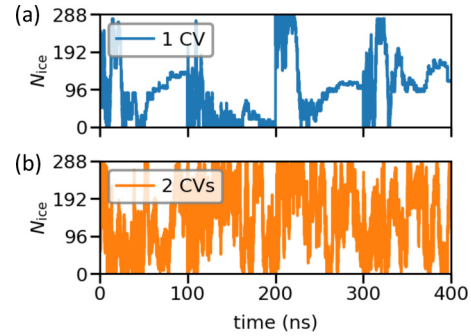

FIG. 2. Evolution of N_{ice} as a function of simulation time for a TIP4P/2005 water system consisting of 288 molecules at 270 K, using the OPES-explore approach with bias applied to (a) only one CV (N_{ice}) and (b) two CVs (N_{ice} and s_2). Note that the data from four multiple walkers are concatenated and presented in a single picture.

with parameters $n = 12$ and $m = 24$ governing the transition behavior [33].

One key feature of this CV is that it enforces a specific lattice orientation during the ice crystallization process. We note that it has achieved success in studying the phase transition between liquid water and ice under the TIP4P/Ice water model [33], as well as in the *ab initio* MD simulations using SCAN functional and machine learning potentials [34]. However, our preliminary simulations of TIP4P/2005 water system with 288 molecules show that, when driven solely by this CV, the transition frequencies between water and ice basins are too low to ensure sufficient sampling and the convergence of thermodynamic properties [Fig. 2(a)]. This indicates that the barrier between the solid and liquid phases is not sufficiently removed by the bias of N_{ice}.

Therefore, we introduce another CV as the translational entropy s_2, which has proven powerful in driving the homogeneous nucleation processes [35,55–57]. It is formulated as a function of the instantaneous radial distribution function $g(r)$ of oxygen-oxygen,

$$s_2 = -2\pi\rho k_{\text{B}}\int_0^{r_{\max}}[g(r)\ln g(r) - g(r) + 1]r^2 dr, \tag{13}$$

where ρ is the density of the system and $r_{\max}$ is the upper limit of the radial distance integration, set to 5 Å. The addition of CV s_2 leads to a noticeable increase in the transition frequencies, as shown in Fig. 2(b). Thus we use both N_{ice} and s_2 to conduct all the OPES-explore simulations.

D. Computational details

All the OPES-explore simulations were carried out using the LAMMPS software [58] interfaced with PLUMED [59]. For all NpT simulation employing the TIP4P/2005 water potential, T and p were maintained using the Nóse-Hoover thermostat and barostat [60,61], with relaxation times of 0.1 ps and 1 ps. A time step of 1 fs was used. The cutoff for the Lennard-Jones and Coulomb interactions was set as 9 Å, while the long-range Coulomb interactions were computed with the particle-particle particle-mesh (PPPM) solver [62] in the reciprocal space at an accuracy of 10^{-6}. Tail corrections to the energy and pressure were added to include the long-

range van der Waals interactions [63]. The bond lengths and angles of water were fixed using the SHAKE algorithm [64]. For simulations employing the mW water potential, we used relaxation times of 0.5 ps for T control and 5 ps for p control, with a 5 fs integration time step.

To accelerate the convergence of sampling, the OPES-explore simulations were performed using four walkers [65]. Each walker was equilibrated for at least 50 ns. The bias potential was updated every 0.5 ps. The approximate free-energy barriers to be overcome for systems of 256, 288, and 384 molecules were all set to 200 kJ/mol. The bias factors for the target well-tempered distributions were automatically determined based on the predefined barrier heights [48]. In addition to the primary CVs promoting the formation of ice Ih, we employ two extra CVs to prevent the emergence of undesirable configurations, i.e., structures misaligned with the prescribed lattice orientation and those corresponding to the cubic ice (Ic) phase, as detailed in Ref. [33].

We use a descriptor defined by the free-energy difference between liquid water and ice to evaluate the convergence of sampling. It is calculated for all the sampled configurations as

$$\Delta F = -\frac{1}{\beta}\ln\left(\frac{P_{\text{ice}}}{1-P_{\text{ice}}}\right), \tag{14}$$

where P_{ice} is the probability of configurations being in the ice phase. This P_{ice} is computed by counting the number of configurations (after reweighting) with N_{ice} larger than a threshold N_{th}, which distinguishes ice states from liquid water. Theoretically, N_{th} should correspond to the dividing surface that separates the reactant and product regions, while, in practice, the value of ΔF is largely insensitive to the choice of N_{th}, as configurations with high free-energy contribute minimally to P_{ice}. Thus $N_{\text{th}} = N/2$ is used for simplicity [33].

III. RESULTS AND DISCUSSIONS

A. TIP4P/2005 water model

We start with the OPES-explore simulation of 288 water molecules at 270 K and 1 bar using the TIP4P/2005 water potential. The system was constructed in an orthorhombic simulation box of 23.37 Å × 21.96 Å × 18.0 Å, generated through a 3 × 3 × 2 replication of the ice Ih unit cell. Figure 3(a) demonstrates the convergence of free energy differences (ΔF) across four independent 50 ns walker trajectories. The plateau reached after ~50 ns confirms the sufficient sampling for Lee-Yang zeros analysis. The corresponding reweighted probability distribution of enthalpy computed from the complete trajectory is presented in Fig. 3(b). Double peaks, representing ice (lower H) and liquid (higher H), highlight a pronounced stability difference between the two phases, with the liquid phase being notably predominant at 270 K.

The roots y_k^*, referred to as y zeros derived from Eq. (9), lie primarily on a circle in the complex plane with a radius much smaller than 1, as shown in Fig. 3(c). Due to the deviations of H from a normal distribution caused by statistical errors, which is inherent in the numerical sampling techniques like MD or MC, some roots also lie outside or inside this circle. Using the relation $y = e^{-(\tilde{\beta}-\beta)\Delta H}$, one can convert the y zeros

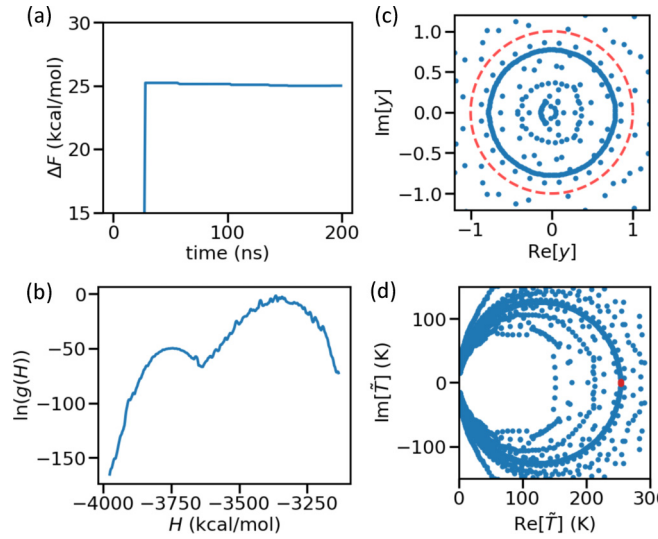

FIG. 3. (a) Convergence of ΔF as a function of simulation time. (b) The probability distribution of H reweighted from the total 200 ns trajectory of four walkers. The bin size ΔH is set to 2 kcal/mol. (c) The distribution of zeros of the partition function expressed in polynomial form in Eq. (9). The red dashed curve represents a unit circle centered at the origin. (d) Lee-Yang zeros in the complex T plane. The red points highlighted refer to the zeros closest to the real axis. The distribution of zeros displays a symmetric pattern about the real axis. All data are obtained for the TIP4P/2005 water model.

to $\tilde{T}$ zeros, i.e., the zeros on the complex plane of temperature, as shown in Fig. 3(d). The $\tilde{T}$ zeros closest to the real axis, referred to as the $\tilde{T}$ edges (denoted by red points), are located at $253.35 \pm 1.10i$ K. The real part of $\tilde{T}$ edges corresponds to the melting temperature, while the imaginary part reflects the "offset" from the thermodynamic limit, associated with the fact that a finite size of the simulation cell is used. Remarkably, this approach enables accurate determination of the phase transition temperature, even when simulations are conducted at temperatures distant from the actual melting point.

In Ref. [17], the Lee-Yang unit circle theorem was proposed for $y \sim e^{\mu/(k_B T)}$, which, according to their discussions, is applicable for a wide range of interatomic and intermolecular interactions. Our numerical simulations of the roots $y = e^{-(\tilde{\beta}-\beta)\Delta H}$ for the phase transition between liquid water and ice confirm the circular distribution predicted by this theorem, as clearly shown in Fig. 3(c). While the thermodynamic state is naturally described by temperature T rather than y, Fig. 3(d) reveals that the $\tilde{T}$ zeros also exhibit an approximately circular distribution. To understand this, we assume the y zeros in the complex plane as $y^* = r\,e^{i\theta}$, with r being the radius. Through this mapping, we mathematically derive that the $\tilde{T}$ zeros must lie on a circle, centered at $T_0/2$ with a radius $T_0/[2(1 - k_B T_0 \ln r/\Delta H)]$, where T_0 is the target temperature of the NpT simulation. Being on the right boundary of this circle, the real part of the $\tilde{T}$ edges can be approximately expressed as

$$\text{Re}[\tilde{T}\text{ edges}] = \frac{T_0}{2} + \frac{T_0}{2(1 - k_B T_0 \ln r/\Delta H)}. \tag{15}$$

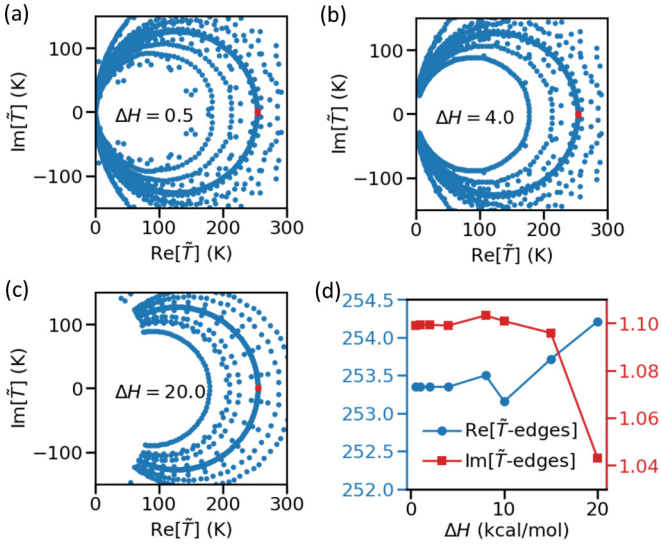

FIG. 4. Distributions of $\tilde{T}$ zeros with bin sizes of (a) $\Delta H = 0.5$ kcal/mol, (b) $\Delta H = 4$ kcal/mol, and (c) $\Delta H = 20$ kcal/mol, for the TIP4P/2005 water system. (d) The real and imaginary parts of the $\tilde{T}$ edges as a function of ΔH, represented by blue circles and red squares, respectively.

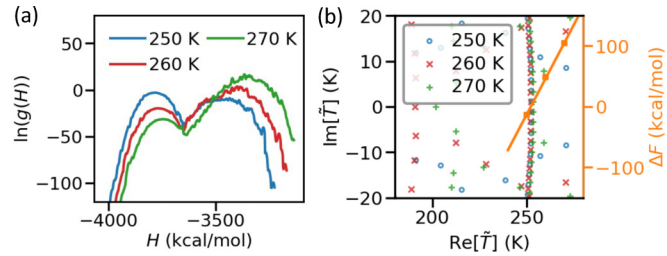

FIG. 5. (a) Enthalpy probability distribution obtained from the OPES-explore simulations of the TIP4P/2005 water system conducted at 250 K, 260 K, and 270 K. (b) A subset of $\tilde{T}$ zeros calculated from the simulations of the TIP4P/2005 water system at 250 K (blue hollow circles), 260 K (red crosses), and 270 K (green plus signs). The orange squares and line represent the linear fit to the ΔF values obtained from simulations at different temperatures.

However, one can still see subtle deviations from a circle shape in Fig. 3(d). A detailed discussion of the physical meanings of these zeros' features, analyzed through Gaussian distribution models, is provided in Appendix B.

It is worth mentioning that the number of bins discretizing H equals the number of y zeros, according to Eq. (9). Consequently, a smaller bin size will lead to a denser distribution of zeros. To assess the influence of bin size on the distribution of Lee-Yang zeros, we vary ΔH across a range of values from 0.5 to 20 kcal/mol, with results shown in Fig. 4. For $\Delta H \leqslant 4$ kcal/mol, the $\tilde{T}$-zeros distributions exhibit good consistency [Figs. 4(a) and 4(b)] and, crucially, the variation in $\tilde{T}$ edges remains well within the statistical uncertainties [Fig. 4(d)], reinforcing the robustness of this approach. However, increasing ΔH to 15 kcal/mol induces noticeable deviations in both the real and imaginary components of the $\tilde{T}$ edges. Such large ΔH values should be avoided, as they result in excessively coarse estimations of $g(H)$ and, consequently, the partition function.

To ensure numerical stability of this scheme, we perform OPES-explore simulations at target T's of 250 K and 260 K, in addition to 270 K, under the same p (1 bar). The resulting probability distributions of H at these temperatures are compared in Fig. 5(a). As T decreases, the probability of configurations being in the liquid phase drops by several orders of magnitude, while the probability of ice phase significantly increases. Despite the distinct H distributions, the $\tilde{T}$ zeros shown in Fig. 5(b) show highly consistent behaviors across these simulations. Specifically, the $\tilde{T}$ edges obtained at 250 K, 260 K, and 270 K are located at $252.42 \pm 1.17i$ K, $252.13 \pm 1.07i$ K, and $253.35 \pm 1.10i$ K, respectively. This demonstrates that the melting temperature, determined from Lee-Yang zeros, is basically insensitive to the target T of the NpT simulation, as long as the probability distribution of H is well sampled. In general, one could determine the phase boundary within a single simulation by using OPES or other enhanced sampling methods, without prior knowledge of the approximate transition temperature range. This scheme enables an efficient exploration of the phase diagram without experimental inputs or artificial supervision, making it suitable for high-throughput calculations.

For direct comparison with conventional free energy methods, we perform a linear fit to the ΔF's obtained at 250 K, 260 K, and 270 K [orange line in Fig. 5(b)]. The melting T can also be determined from the point where $\Delta F = 0$, yielding 252.13 K. This result demonstrates excellent agreement between the melting temperatures obtained from the Lee-Yang method and the free energy approach.

B. mW water model

To deduce the phase boundary in the thermodynamic limit, we employ the mW water potential to investigate the system-size dependence. After testing a series of box sizes, we observe that the melting points for systems with the same number of water molecules but different lattice orientations (e.g., $N = 256$ with $2 \times 2 \times 4$, $2 \times 4 \times 2$, and $4 \times 2 \times 2$ geometries) exhibit minor variations once N is sufficiently large. The specific values of the $\tilde{T}$ edge for each geometry at $N = 256$, $N = 288$, and $N = 384$ are summarized in Table I.

TABLE I. Calculated $\tilde{T}$-edge values for mW water systems with $N = 256$, 288, and 384 under different lattice orientations. Each block represents a 200 ns trajectory simulated with four walkers at 270 K.

N	Geometry	Block 1	Block 2	Block 3
256	$2 \times 2 \times 4$	$281.44 \pm 1.68i$	$282.46 \pm 1.59i$	$281.55 \pm 1.56i$
	$2 \times 4 \times 2$	$282.08 \pm 1.64i$	$282.50 \pm 1.61i$	$282.68 \pm 1.61i$
	$4 \times 2 \times 2$	$281.16 \pm 1.60i$	$282.84 \pm 1.59i$	$281.87 \pm 1.57i$
288	$2 \times 3 \times 3$	$280.91 \pm 1.38i$	$281.00 \pm 1.42i$	$280.74 \pm 1.42i$
	$3 \times 2 \times 3$	$280.70 \pm 1.37i$	$281.44 \pm 1.42i$	$280.58 \pm 1.39i$
	$3 \times 3 \times 2$	$280.79 \pm 1.40i$	$281.21 \pm 1.33i$	$282.09 \pm 1.42i$
384	$2 \times 4 \times 3$	$280.52 \pm 1.05i$	$280.29 \pm 1.04i$	$279.38 \pm 1.04i$
	$4 \times 2 \times 3$	$279.64 \pm 1.04i$	$279.63 \pm 1.03i$	$279.39 \pm 1.06i$
	$4 \times 3 \times 2$	$279.62 \pm 1.06i$	$279.35 \pm 1.02i$	$278.49 \pm 1.02i$

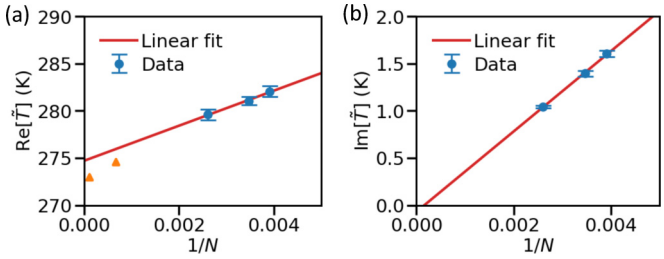

FIG. 6. (a) Real part and (b) the imaginary part of $\tilde{T}$ edges as a function of inverse system size, obtained using the mW water potential. Error bars represent variations across the three distinct lattice geometries listed in Table I. The orange triangles denote the melting temperatures obtained from the coexistence method using the same mW potential, as reported in Refs. [50,67].

As the melting point becomes isotropic in sufficiently large systems, we can determine the thermodynamic limit using the orientation-averaged values of $\tilde{T}$ edges. As shown in Fig. 6, both the real and imaginary components of the averaged $\tilde{T}$ edges exhibit linear scaling with $1/N$, in alignment with the finite-size scaling predictions for first-order phase transitions [66]. Through linear fitting, the real part of the $\tilde{T}$ edges approaches a melting temperature of 274.70 K in the thermodynamic limit, which agrees closely with previously reported values of 274.6 K (for an ∼1500-water system) [50] and 273.0 K (for an ∼9000-water system) [67] obtained via the phase coexistence method (orange triangles in Fig. 6). Meanwhile, the imaginary component effectively diminishes in the thermodynamic limit, as expected for a first-order transition.

IV. CONCLUSIONS

We apply the Lee-Yang phase transition theory to determine the melting temperature of ice Ih by integrating the enhanced sampling method. To ensure proper sampling of phase space, we conduct OPES-explore simulations using two CVs, i.e., the number of ice-like molecules N_{ice} and the translational entropy s_2. Using the TIP4P/2005 water model, the $\tilde{T}$ zeros of the partition function are derived from the reweighted enthalpy probability distributions. Notably, the zeros closest to the real axis ($\tilde{T}$ edges) show remarkable insensitivity to the target T of the NpT simulation and the bin size ΔH. Extrapolation to the thermodynamic limit for the mW water model yields a melting temperature of 274.70 K, showing excellent agreement with previous studies. This work underscores the robustness of the Lee-Yang method, which arises from the inherent equivalence between Lee-Yang zeros and the partition function. Furthermore, we highlight its superior efficiency, as only a single simulation is required, in contrast to traditional methods that rely on multiple coexistence or heating/cooling simulations. We anticipate this scheme to have wide-ranging applications across a variety of realistic systems.

ACKNOWLEDGMENTS

This work is supported by the National Science Foundation of China under Grants No. 12204015, No. 12234001, No. 12474215, and No. 62321004, the National Basic Research Program of China under Grants No. 2021YFA1400500 and No. 2022YFA1403500, and the China Postdoctoral Science Foundation under Grants No. 2025M773371 and No. GZC20252222. We thank the supercomputer center at Peking University for computational resources.

DATA AVAILABILITY

The data are available from the authors upon reasonable request.

APPENDIX A: PYTHON SCRIPT FOR CALCULATING $\tilde{T}$ ZEROS

This appendix outlines the procedure for calculating polynomial roots of partition function and the zeros, which can be readily implemented in a PYTHON code.

ALGORITHM 1. Calculating polynomial roots and $\tilde{T}$ zeros.

Input: File "histo" containing probability density data
Output: Generate polynomial roots and temperature zeros
Initialize variables
$dH \leftarrow 2$ ▷ Bin size of energy (kcal/mol)
$T_0 \leftarrow 270$ ▷ Simulated temperature (K)
Load probability density file
$H \leftarrow$ np.loadtxt("histo")
Calculate roots of the polynomial
$roots \leftarrow$ np.polynomial.polynomial.polyroots(H[:, 1])
$X \leftarrow \mathrm{Re}(roots)$
$Y \leftarrow \mathrm{Im}(roots)$
Calculate temperature zeros
$ln_values \leftarrow \mathrm{np.log}(roots) + 2k\pi i$
$Beta_zeros \leftarrow -ln_values/dH + 1/(k_{\mathrm{B}} \times T_0)$
$T_zeros \leftarrow 1/(Beta_zeros \times k_{\mathrm{B}})$
$Tx \leftarrow \mathrm{Re}(T_zeros)$
$Ty \leftarrow \mathrm{Im}(T_zeros)$

APPENDIX B: GEOMETRICAL CORRELATIONS BETWEEN THE ENTHALPY DISTRIBUTION AND ZEROS

In the practice of calculating zeros, one might observe more zeros approaching the real axis than the one related to phase transition. Here, we shall demonstrate that these additional zeros rise from limited sampling resolution and are thus unphysical. In the NpT ensemble, the H probability $g_\beta(H)$ observed at $T = \beta^{-1}$ can be scaled from a reference $g_{\beta_0}(H)$ at $T_0 = \beta_0^{-1}$ by an exponential factor $e^{-(\beta-\beta_0)H}$. To provide an intuitive understanding, we employ a geometrical explanation. When the $g_\beta(H)$ is plotted on a logarithm scale, this factor manifests as a tilted temperature axis. Since the choice of T_0 is arbitrary, we consider an example where T_0 is near the phase transition temperature, at which $g(H)$ exhibits a double peak line shape, as shown by the blue curve in Fig. 7(a). Correspondingly, the calculated zeros form three branches, as shown by y zeros in Fig. 7(b) and $\tilde{T}$ zeros in Fig. 7(c). The central branch, denoted as $T_{\mathrm{pt}}(y_{\mathrm{pt}})$, corresponds to the target phase transition, while the left and right one, termed by $T_{\mathrm{l}}(y_{\mathrm{l}})$ and $T_{\mathrm{r}}(y_{\mathrm{r}})$, are unphysical.

In this geometrical framework, the original T axis is horizontal, aligned with β_0, but it tilts to a slope corresponding to β_i at T_i. The interplay between the tilted T axis and the

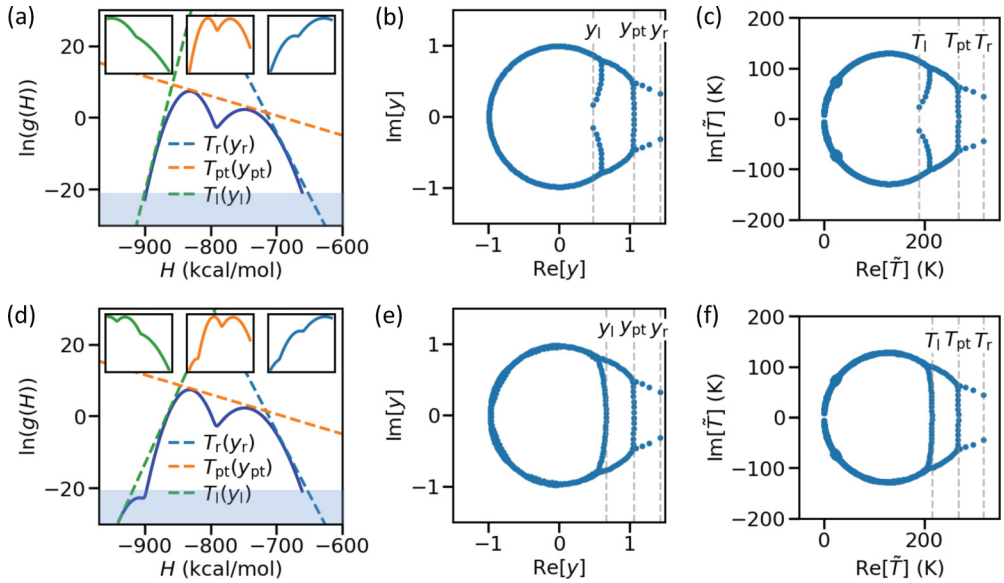

FIG. 7. (a) Schematic plot of the probability distribution of enthalpy, modeled with two Gaussian functions representing the ice and liquid water phases, respectively. The cyan, orange, and green dashed lines denote the titled temperature axes. The insets display the rescaled H distribution after reweighting to the target T or y. The blue shadow depicts the area below the resolution threshold. Panels (b) and (c) show the distribution of y zeros and $\tilde{T}$ zeros. $T_l(y_l)$ and $T_r(y_r)$ are the real parts of the left and right branch, respectively, while $T_{pt}(y_{pt})$ denotes the phase transition point. Panels (d)–(f) correspond to (a)–(c), but include a subtle peak below the original sampling resolution. In (e) and (f), the left branch of zeros shift closer to the real axis compared to (b) and (c), signaling a new phase transition.

$g(H)$ line shape provides insights into the behavior of zeros. When the tilted T axis is tangent to both peaks, the slope exactly maps to the transition temperature T_{pt}, as shown as orange lines in Fig. 7(a). Below and above this T_{pt}, the tilted axis is tangent to either the left or right peak, respectively. We represent the temperatures at the edges of the left and right branches of zeros, i.e., T_l and T_r, with green and cyan dashed lines, respectively. T_l and T_r appear to be the end points beyond which the axis intersects with the line shape of $g(H)$ instead of being tangent to it. The reweighted $g(H)$ for T_l, T_{pt}, and T_r are plotted in the insets of Fig. 7(a). As the temperature increases, the line shape switches between a single dominant peak and double peaks, reflecting that the system experiences a phase transition. Thus we connect the tangent behavior with the positions of edge zeros.

However, sampling techniques inherently overlook configurations with probabilities significantly below the resolution threshold. In primitive sampling, the sample size N determines that configurations with probability much less than N^{-1} are rarely sampled, while in enhanced sampling methods configurations with $p \ll c \cdot N^{-1}$ are still out of reach, even though the efficiency has been enhanced by a factor of c. This limitation is particularly pronounced on a logarithm scale. In fact, additional peaks may exist below the resolution threshold and are undetected. For example, as shown in Fig. 7(d), one would perceive a new peak when the sampling was enhanced by ten orders of magnitude. Before the axis tilts to T_l, it becomes tangent to both the new peak and original left peak. Correspondingly, we observe that the zeros shift closer to the real axis, indicating a real phase transition, while T_{pt} and T_r remain unchanged [Figs. 7(e) and 7(f)]. Therefore, the edges of the left and right branches in Figs. 7(b) and 7(c) are a consequence of insufficient information below the sampling resolution. Only by accounting for more subtle configurations can one reveal physically meaningful results, such as the occurrence of a phase transition.

[1] P. W. Anderson, More is different, Science **177**, 393 (1972).
[2] M. K. Wu, J. R. Ashburn, C. J. Torng, P. H. Hor, R. L. Meng, L. Gao, Z. J. Huang, Y. Q. Wang, and C. W. Chu, Superconductivity at 93 K in a new mixed-phase Y-Ba-Cu-O compound system at ambient pressure, Phys. Rev. Lett. **58**, 908 (1987).
[3] P. G. Debenedetti and F. H. Stillinger, Supercooled liquids and the glass transition, Nature (London) **410**, 259 (2001).
[4] D. D. Fong, G. B. Stephenson, S. K. Streiffer, J. A. Eastman, O. Auciello, P. H. Fuoss, and C. Thompson, Ferroelectricity in ultrathin perovskite films, Science **304**, 1650 (2004).
[5] B. A. Bernevig, T. L. Hughes, and S.-C. Zhang, Quantum spin Hall effect and topological phase transition in HgTe quantum wells, Science **314**, 1757 (2006).
[6] S. Sachdev, Quantum magnetism and criticality, Nat. Phys. **4**, 173 (2008).
[7] J. Carrasquilla and R. G. Melko, Machine learning phases of matter, Nat. Phys. **13**, 431 (2017).

[8] Q.-J. Ye, Z.-Y. Liu, Y. Feng, P. Gao, and X.-Z. Li, Ferroelectric problem beyond the conventional scaling law, Phys. Rev. Lett. **121**, 135702 (2018).

[9] H. Stanley, *Introduction to Phase Transitions and Critical Phenomena*, International Series of Monographs on Physics (Oxford University Press, Oxford, 1987).

[10] J. D. van der Waals, Over de Continuïteit van den Gas - en Vloeistoftoestand (On the continuity of the gaseous and liquid states), Ph.D. thesis, Universiteit Leiden, Leiden, Netherlands, 1873.

[11] J. W. Gibbs, On the equilibrium of heterogeneous substances, Trans. Conn. Acad. Arts Sci. **3**, 108 (1875-1878).

[12] L. Pauling, *The Nature of the Chemical Bonding* (Cornell University Press, Ithaca, NY, 1960).

[13] W. Lenz, Beitrag zum verständnis der magnetischen erscheinungen in festen körpern, Z. Phys. **21**, 613 (1920).

[14] E. Ising, Beitrag zur Theorie des Ferromagnetismus (Contribution to the theory of ferromagnetism), Z. Phys. **31**, 253 (1925).

[15] L. Onsager, Crystal statistics. I. A two-dimensional model with an order-disorder transition, Phys. Rev. **65**, 117 (1944).

[16] C. N. Yang and T. D. Lee, Statistical theory of equations of state and phase transitions. I. Theory of condensation, Phys. Rev. **87**, 404 (1952).

[17] T. D. Lee and C. N. Yang, Statistical theory of equations of state and phase transitions. II. Lattice gas and Ising model, Phys. Rev. **87**, 410 (1952).

[18] M. E. Fisher, *Lectures in Theoretical Physics* (University of Colorado Press, Boulder, CO, 1965), Vol. 7C.

[19] C. Flindt and J. P. Garrahan, Trajectory phase transitions, Lee-Yang zeros, and high-order cumulants in full counting statistics, Phys. Rev. Lett. **110**, 050601 (2013).

[20] A. Deger and C. Flindt, Determination of universal critical exponents using Lee-Yang theory, Phys. Rev. Res. **1**, 023004 (2019).

[21] P. M. Vecsei, J. L. Lado, and C. Flindt, Lee-Yang theory of the two-dimensional quantum Ising model, Phys. Rev. B **106**, 054402 (2022).

[22] J. Lee, Exact partition function zeros of the Wako-Saitô-Muñoz-Eaton protein model, Phys. Rev. Lett. **110**, 248101 (2013).

[23] W. van Dijk, C. Lobo, A. MacDonald, and R. K. Bhaduri, Fisher zeros of a unitary Bose gas, Can. J. Phys. **93**, 830 (2015).

[24] K. P. Gnatenko, A. Kargol, and V. M. Tkachuk, Two-time correlation functions and the Lee-Yang zeros for an interacting Bose gas, Phys. Rev. E **96**, 032116 (2017).

[25] D. Frenkel and B. Smit, *Understanding Molecular Simulation: From Algorithms to Applications* (Elsevier, Amsterdam, 2002).

[26] B. J. Alder and T. E. Wainwright, Molecular dynamics by electronic computers, in *Proceedings of the International Symposium on Transport Processes in Statistical Mechanics* (Interscience, Brussels, 1958), pp. 97–131.

[27] G. Battimelli and G. Ciccotti, Berni Alder and the pioneering times of molecular simulation, Eur. Phys. J. H **43**, 303 (2018).

[28] N. Metropolis, A. W. Rosenbluth, M. N. Rosenbluth, A. H. Teller, and E. Teller, Equation of state calculations by fast computing machines, J. Chem. Phys. **21**, 1087 (1953).

[29] D. Frenkel, Introduction to Monte Carlo methods, *Computational Soft Matter: From Synthetic Polymers to Proteins*, Lecture Notes, NIC Series, Vol. 23 (John von Neumann Institute for Computing, Julich, 2004), p. 29.

[30] R. Car and M. Parrinello, Unified approach for molecular dynamics and density-functional theory, Phys. Rev. Lett. **55**, 2471 (1985).

[31] R. Iftimie, P. Minary, and M. E. Tuckerman, *Ab initio* molecular dynamics: Concepts, recent developments, and future trends, Proc. Natl. Acad. Sci. USA **102**, 6654 (2005).

[32] D. Frenkel and B. M. Mulder, The hard ellipsoid-of-revolution fluid, Mol. Phys. **55**, 1171 (1985).

[33] P. M. Piaggi and R. Car, Phase equilibrium of liquid water and hexagonal ice from enhanced sampling molecular dynamics simulations, J. Chem. Phys. **152**, 204116 (2020).

[34] P. M. Piaggi, A. Z. Panagiotopoulos, P. G. Debenedetti, and R. Car, Phase equilibrium of water with hexagonal and cubic ice using the SCAN functional, J. Chem. Theory Comput. **17**, 3065 (2021).

[35] T. E. Gartner, P. M. Piaggi, R. Car, A. Z. Panagiotopoulos, and P. G. Debenedetti, Liquid-liquid transition in water from first principles, Phys. Rev. Lett. **129**, 255702 (2022).

[36] M. Yang, T. Karmakar, and M. Parrinello, Liquid-liquid critical point in phosphorus, Phys. Rev. Lett. **127**, 080603 (2021).

[37] D. Alfè, First-principles simulations of direct coexistence of solid and liquid aluminum, Phys. Rev. B **68**, 064423 (2003).

[38] M. M. Conde, M. Rovere, and P. Gallo, High precision determination of the melting points of water TIP4P/2005 and water TIP4P/Ice models by the direct coexistence technique, J. Chem. Phys. **147**, 244506 (2017).

[39] S. Blazquez and C. Vega, Melting points of water models: Current situation, J. Chem. Phys. **156**, 216101 (2022).

[40] L.-F. Zhu, J. Janssen, S. Ishibashi, F. Körmann, B. Grabowski, and J. Neugebauer, A fully automated approach to calculate the melting temperature of elemental crystals, Comput. Mater. Sci. **187**, 110065 (2021).

[41] C. J. Pickard, M. Martinez-Canales, and R. J. Needs, Density functional theory study of phase IV of solid hydrogen, Phys. Rev. B **85**, 214114 (2012).

[42] J. Chen, X. Ren, X.-Z. Li, D. Alfè, and E. Wang, On the room-temperature phase diagram of high pressure hydrogen: An *ab initio* molecular dynamics perspective and a diffusion Monte Carlo study, J. Chem. Phys. **141**, 024501 (2014).

[43] J. C. S. Rocha, S. Schnabel, D. P. Landau, and M. Bachmann, Identifying transitions in finite systems by means of partition function zeros and microcanonical inflection-point analysis: A comparison for elastic flexible polymers, Phys. Rev. E **90**, 022601 (2014).

[44] B. Costa, L. Mól, and J. Rocha, Energy probability distribution zeros: A route to study phase transitions, Comput. Phys. Commun. **216**, 77 (2017).

[45] X.-Y. Ouyang, Q.-J. Ye, and X.-Z. Li, Complex phase diagram and supercritical matter, Phys. Rev. E **109**, 024118 (2024).

[46] This H should be distinguished from the thermodynamic enthalpy $\langle H \rangle$ in statistical mechanics, which is strictly an ensemble-averaged equilibrium property, whereas the instantaneous H is commonly accepted in the molecular simulation community.

[47] J. Palmer, F. Martelli, Y. Liu, R. Car, A. Z. Panagiotopoulos, and P. G. Debenedetti, Metastable liquid–liquid transition in a molecular model of water, Nature (London) **510**, 385 (2014).

[48] M. Invernizzi and M. Parrinello, Exploration vs convergence speed in adaptive-bias enhanced sampling, J. Chem. Theory Comput. **18**, 3988 (2022).
[49] J. L. F. Abascal and C. Vega, A general purpose model for the condensed phases of water: TIP4P/2005, J. Chem. Phys. **123**, 234505 (2005).
[50] V. Molinero and E. B. Moore, Water modeled as an intermediate element between carbon and silicon, J. Phys. Chem. B **113**, 4008 (2009).
[51] M. Matsumoto, T. Yagasaki, and H. Tanaka, GenIce: Hydrogen-disordered ice generator, J. Comput. Chem. **39**, 61 (2018).
[52] M. Matsumoto, T. Yagasaki, and H. Tanaka, GenIce-core: Efficient algorithm for generation of hydrogen-disordered ice structures, J. Chem. Phys. **160**, 094101 (2024).
[53] P. M. Piaggi and M. Parrinello, Calculation of phase diagrams in the multithermal-multibaric ensemble, J. Chem. Phys. **150**, 244119 (2019).
[54] P. M. Piaggi, "Environment finder: A tool for finding and analyzing atomic environments in crystal structures", Zenodo (2021), doi:10.5281/zenodo.4746325.
[55] P. M. Piaggi, O. Valsson, and M. Parrinello, Enhancing entropy and enthalpy fluctuations to drive crystallization in atomistic simulations, Phys. Rev. Lett. **119**, 015701 (2017).
[56] P. M. Piaggi and M. Parrinello, Predicting polymorphism in molecular crystals using orientational entropy, Proc. Natl. Acad. Sci. USA **115**, 10251 (2018).
[57] H. Niu, Y. I. Yang, and M. Parrinello, Temperature dependence of homogeneous nucleation in ice, Phys. Rev. Lett. **122**, 245501 (2019).
[58] A. P. Thompson, H. M. Aktulga, R. Berger, D. S. Bolintineanu, W. M. Brown, P. S. Crozier, P. J. in 't Veld, A. Kohlmeyer, S. G. Moore, T. D. Nguyen, R. Shan, M. J. Stevens, J. Tranchida, C. Trott, and S. J. Plimpton, LAMMPS - a flexible simulation tool for particle-based materials modeling at the atomic, meso, and continuum scales, Comput. Phys. Commun. **271**, 108171 (2022).
[59] G. A. Tribello, M. Bonomi, D. Branduardi, C. Camilloni, and G. Bussi, PLUMED 2: New feathers for an old bird, Comput. Phys. Commun. **185**, 604 (2014).
[60] S. Nosé, A unified formulation of the constant temperature molecular dynamics methods, J. Chem. Phys. **81**, 511 (1984).
[61] W. G. Hoover, Canonical dynamics: Equilibrium phase-space distributions, Phys. Rev. A **31**, 1695 (1985).
[62] R. W. Hockney and J. W. Eastwood, *Computer Simulation Using Particles* (CRC Press, Boca Raton, FL, 1988).
[63] H. Sun, COMPASS: An *ab initio* force-field optimized for condensed-phase applications–overview with details on alkane and benzene compounds, J. Phys. Chem. B **102**, 7338 (1998).
[64] J.-P. Ryckaert, G. Ciccotti, and H. J. Berendsen, Numerical integration of the Cartesian equations of motion of a system with constraints: Molecular dynamics of n-alkanes, J. Comput. Phys. **23**, 327 (1977).
[65] P. Raiteri, A. Laio, F. L. Gervasio, C. Micheletti, and M. Parrinello, Efficient reconstruction of complex free energy landscapes by multiple walkers metadynamics, J. Phys. Chem. B **110**, 3533 (2006).
[66] K. Binder, Theory of first-order phase transitions, Rep. Prog. Phys. **50**, 783 (1987).
[67] A. Hudait, S. Qiu, L. Lupi, and V. Molinero, Free energy contributions and structural characterization of stacking disordered ices, Phys. Chem. Chem. Phys. **18**, 9544 (2016).